AIAA JOURNAL
Vol. 46, No. 5, May 2008

Two-Dimensional Simulation of Stripping Breakup of a Water Droplet

H. Chen
Leader University, Tainan City 70970, Taiwan, Republic of China

DOI: 10.2514/1.31286

The breakup of a liquid droplet induced by a high-speed gas stream is a known multiphase flow problem. Among various breakup modes of liquid droplets impinged by shock waves, the stripping breakup takes place over a wide range of Weber numbers, from 100 to approximately 20,000. In this study, the evolution of the stripping breakup of a water droplet is simulated by using a multiphase flow solver with a five-equation model. Several test cases such as gas–gas shock tube, water–air shock tube, and underwater explosion problems are performed to validate the present numerical methods. To compare with the experimental results, the water droplets with diameters of 6.4 and 4.8 mm and Mach numbers of 1.3 and 1.47 are chosen in this study. The stripping breakup of a water droplet, including the shape deformation, vortex shedding, unsteady drag force, and flow instability, is investigated. The computed displacement, acceleration, and volume change of the water droplet are in agreement with the experimental data in dimensionless form. The evolution of a water droplet during the stripping breakup for an inviscid flow is presented by flow visualization.

I. Introduction

THE breakup of a liquid droplet induced by a high-speed gas stream is a known multiphase flow problem. This problem has many engineering and scientific applications such as damage caused by rain droplets impinging on aircraft in a high-speed flight, combustion and detonation in multiphase mixtures, ablation of space vehicles during an atmosphere reentry, fuel–coolant interaction in light water reactors, and sodium–water reaction in steam generators of fast breeder reactors, etc. As a result, the breakup of a liquid droplet has been extensively studied by many researchers. The comprehensive reviews of droplet breakup were proposed by Wierzba and Takayama [1] and by Joseph et al. [2]. However, the mechanism of the three-dimensional droplet breakup is still unclear.

Basically, the types of liquid-droplet breakup according to the value of the Weber number can be classified into six modes [3,4]: vibrational mode, bag mode, bag-and-stamen mode, chaotic mode, stripping (shear) mode, and catastrophic mode. In this study, we will focus on the stripping (shear) breakup of a water droplet. Among various breakup modes of liquid droplets impinged by shock waves, the stripping breakup takes place over a wide range of Weber numbers, from 100 to approximately 20,000. Early experimental investigations of the stripping breakup have been proposed by Ranger and Nicholls [5]. They studied shock waves in air moving over a water droplet at Mach numbers of 1.5–3.5. Photographic, drop displacement, and breakup-time information were presented. They also formulated a model for breakup phenomenon by considering that the breakup results from the boundary-layer stripping mechanism. To compute the disintegration rate, the variations of drop shape and drop velocity with time were used together with analytical results. Wierzba and Takayama [1] experimentally studied the deformation and the mechanism of stripping breakup of liquid drops. In their work, water drops with diameters of 1030 and 4300 μm were examined for shock Mach numbers ranging from 1.3 to 1.5 in air. A four-stage mechanism of the stripping breakup of liquid drops was proposed by using holographic interferometry. Joseph et al. [2] studied the breakup of viscous and viscoelastic drops in the high-speed airstream behind a shock wave. Experimental photos were taken by a rotating drum camera every 5 μs. In their work, bag and bag-and-stamen breakups were observed at very high Weber numbers in the regime of breakup previously called catastrophic. Yoshida and Takayama [6] have shown that the patterns of the droplet breakup differed significantly, depending on the method of visualization. Patterns of the droplet's breakup observed by double-exposure image holographic interferometry were found to be different from those observed by shadowgraphs. Chou et al. [7] experimentally studied the temporal properties of drop breakup in the shear breakup regime by using shadowgraphy and holography. Their test conditions included various parameters of the Weber number from 125 to 375, Ohnesorge number from 0.003 to 0.04, liquid/gas density ratio from 670 to 990, and Reynolds number from 3000 to 12,000. From their shadowgraphs, ligaments were observed to be stripped from the boundary layer at the periphery of the original drop. The boundary layer was developed along the surface on the upstream side of the drop. In addition, they mentioned that the drop size formed from the ligament breakup mainly depends on the liquid viscosity. Theofanous et al. [8] presented experimental results of the interfacial instabilities and breakup of Newtonian liquid drops suddenly exposed to a rarefied, high-speed (Mach number 3) airflow. They observed the interfacial phenomena and mixing through the breakup cycle over the range of Weber numbers from 26 to 2600.

Because the shock/droplet interaction is three-dimensional, it may cause uncertainty in visualizing the breakup process with current flow-visualization techniques such as schlieren images, shadowgraphs, and holographic interferograms. For this reason, Igra and Takayama [9] visualized the two-dimensional shock/water-column interactions in a shock tube by sequential double-exposure holographic interferograms. In their study, the incident shock Mach number was 1.47 and the diameter of the water column was 4.8 mm. They mentioned that a two-dimensional shock/water-column interaction provides the only method for quantitative visualization of wave motions in water. Subsequently, Igra and Takayama [10] studied the shock/water-column interactions by numerical simulation. In their work, the governing equations were the Euler equations for a two-dimensional inviscid flow. The advection terms were solved using the modified cubic-interpolated propagation (CIP) scheme, and finite differences were used for other terms. Their numerical results were compared with their previous experimental results [9]. Later, Igra and Takayama [11] investigated the aerodynamic breakup of a cylindrical water droplet by both

Received 28 March 2007; revision received 7 December 2007; accepted for publication 19 December 2007.

*Assistant Professor, Department of Information Communication. Member AIAA.

experiment and simulation. The incident shock Mach number and the diameter of the water column used in their study were 1.47 and 4.8 mm, respectively. Numerical results were obtained by solving Euler equations with the CIP scheme. Their results showed quantitative agreement for density variation in the gaseous phase, whereas for the liquid phase, numerical density distributions showed only qualitative agreement with experimental results. Igra and Takayama [12] extended their study to shock wave loading on a cylindrical water column. In their experiment, the shock Mach number was 1.3 in air, the water-column diameter was 6.4 mm, and the corresponding Weber number and Reynolds number were 3690 and 95,300, respectively. An upwind total-variation-diminishing scheme coupled with the level set method and an interface correction step was developed to simulate this problem. Good agreement was obtained by comparing the isopycnics of their numerical results with the experimental holographic interferograms up to 55 μs. In addition, a survey of experimental results regarding shock interaction with a water column for various Mach numbers and water-column diameters was presented. They studied the trends of the water-column deformation, displacement, and acceleration by comparing with their previous experimental results in dimensionless terms. They found that the trends of water-column deformation for different cases would lie along a similar line.

Unsteady drag force induced by shock loading on a sphere or a cylinder has been studied by many researchers. Tanno et al. [13] experimentally confirmed the presence of unsteady drag force over a sphere impinged by a planar shock wave. In their study, the unsteady drag force coefficient agreed well between the measurement and numerical simulation. An experimental investigation of two cylindrical water columns subjected to planar shock wave loading was reported by Igra and Takayama [14]. In their study, the diameter of water column and Mach number of the shock wave were the same as the present case of $Ms = 1.47$. They mentioned that at the early stage of the shock wave interaction with a water column, its behavior is similar to that of a solid cylinder because there is no deformation of the water column. Hence, a study of unsteady drag force induced by shock loading on a water column is included in this work. It would be interesting to interpret the initial deformation of a water droplet from the point of view of unsteady drag force.

Although the stripping breakup of a liquid droplet has been studied by many researchers, at present, there is no numerical simulation on the entire evolution of stripping breakup. As found in previous experimental results, the instabilities may occur in the breakup process so that the axisymmetric assumption for governing equations is no longer valid. However, a three-dimensional simulation of this problem would cost a huge computational time. Based on the aforementioned reasons, it would be reasonable to investigate the fundamental mechanisms of the stripping breakup of a liquid droplet by beginning with a two-dimensional simulation. To date, how to establish a robust and correct numerical model to incorporate viscosity into a multifluid solver remains a challenge. Considering these issues, we aim to simulate the two-dimensional stripping breakup of a water droplet by using Euler equations with a five-equation model as a preliminary study. Our simulated results will compare with the results of the two-dimensional experiment of Igra and Takayama [12]. The comparison can be used to evaluate the ability of the present numerical method to solve this problem.

II. Numerical Methods

A. Description of the Physical Problem

The problem to be considered is schematically shown in Fig. 1, where Ms is the incident shock Mach number and D_o is the diameter of the water droplet. In this work, all boundary conditions are the far-field conditions. To avoid the numerical errors reflected from the boundaries, the computational domain is

$$\{(x, y)| -40 \le x \le 110, -50 \le y \le 50\} \text{ mm}$$

and grid points are 1500×1000. The center of the water droplet is located at $(x, y) = (0, 0)$. The initial position of the incident shock is

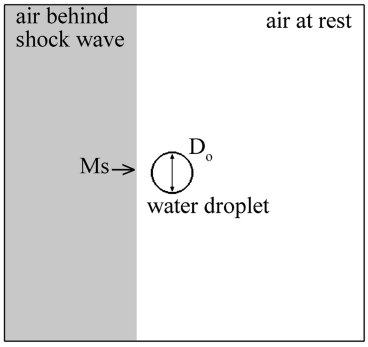

Fig. 1 A schematic diagram for the stripping breakup of a water droplet.

at $x = -4$ mm. To compare with the experimental data of Igra and Takayama [12], $Ms = 1.3$ and 1.47 with the corresponding $D_o =$ 6.4 and 4.8 mm are used in this study. For dimensionless analysis, the following dimensionless parameters are important for liquid-droplet breakup: Weber number We, Ohnesorge number Oh, and Reynolds number Re. The definitions of these parameters are

$$We = \rho_g u_g^2 D_o / \sigma \tag{1}$$

$$Oh = \mu_l / \sqrt{\rho_l \sigma D_o} \tag{2}$$

$$Re = \rho_g u_g D_o / \mu_g \tag{3}$$

where ρ is density, u is the velocity, D_o is the diameter of the liquid droplet, σ is the surface tension, μ is the viscosity, and subscripts l and g represent the liquid and gas behind the shock. The parameters We, Oh, and Re are the ratios of the fluid's inertia force to its surface tension force, viscous force to surface tension force, and inertia force to viscous force, respectively. To compare with the experimental results, the dimensionless parameters are chosen as 3791 and 7473 for We, 0.00146 and 0.00169 for Oh, and 93,995 and 124,884 for Re. These values are based on the corresponding fluid properties, droplet diameters, and Mach numbers. It is noted that these dimensionless parameters are close to the corresponding parameters of Igra and Takayama [12]. Considering the dimensionless analysis, the ratios of all dimensionless parameters are at least greater than $\mathcal{O}(3)$. Therefore, we can conclude that the flow is dominated by inertia force, and it is reasonable to assume that the viscous effect and surface tension are relatively insignificant in this problem. Because direct numerical simulation currently remains a challenging issue, our numerical results can be taken as a milestone for understanding stripping breakup of a water droplet.

To study this problem, a two-dimensional compressible multiphase flow solver with the capability of simulating shock wave interacting with a water droplet is developed. In addition, a diffuse-interface method with a five-equation model [15,16] is adopted. To capture the contact surfaces, an HLLC (Harten–Lax–van Leer scheme for the contact surface) approximate Riemann solver based on the work of Harten et al. [17] and later modified by Toro et al. [18] is chosen. All fluids are governed by the stiffened gas equation of state (EOS). The numerical flux for the conservative flux is computed by a Godunov-type scheme, and the detail of the scheme can be found in the paper of Saurel and Abgrall [19].

B. Five-Equation Model

The diffuse-interface method used here is essentially based on the Eulerian formulation. This method does not describe the interfaces as discontinuities, but as continuous zones. Because of the continuous zone, the transition from one medium to the other is smooth. It is known that using the notion of mass fractions (multispecies algorithm) and partial pressures may result in the pressure and velocity oscillations in a shock tube problem [19]. This is because

both the Euler and Navier–Stokes equations provide a single temperature for the mixture, which forces two fluids to be in a thermal equilibrium even if it is physically impossible. To avoid this error, the notion of volume fractions is adopted.

Saurel and Abgrall [20] proposed that if a two-phase flow is uniform in pressure and velocity on the stencil of the numerical scheme, then the pressure and velocity must stay uniform during its temporal evolution. Based on these assumptions, the two-dimensional equations with a five-equation model for two-phase flows are described as

$$\frac{\partial \alpha}{\partial t} + V \cdot \nabla \alpha = 0 \tag{4a}$$

$$\frac{\partial \alpha_1 \rho_1}{\partial t} + \nabla \cdot (\alpha_1 \rho_1 V) = 0 \tag{4b}$$

$$\frac{\partial \alpha_2 \rho_2}{\partial t} + \nabla \cdot (\alpha_2 \rho_2 V) = 0 \tag{4c}$$

$$\frac{\partial \rho V}{\partial t} + \nabla \cdot (\rho V \otimes V + p) = 0 \tag{4d}$$

$$\frac{\partial \rho E}{\partial t} + \nabla \cdot (V(\rho E + p)) = 0 \tag{4e}$$

where α denotes the volume fraction and $V = [\,u \quad v\,]^T$. Indeed, one EOS is needed to close the preceding five-equation model. There are several choices of EOS for different physical problems such as perfect gas, van der Waals gas [21], Tait gas [22], stiffened-gas, Mie–Grüneisen [23], etc. In this study, the stiffened gas EOS is adopted. The mixture pressure is obtained by Eq. (5):

$$p = (\gamma - 1)\rho e - \gamma \pi \tag{5}$$

where γ denotes the mixture thermodynamic constant and π the mixture reference pressure. The mixture density is given by $\rho = \sum \alpha_i \rho_i$, where subscript i represents the fluid i. Because the pressure equilibrium between fluids is assumed, the mixtures γ and π can be computed by Eqs. (6) and (7), respectively. For this model, the mixture speed of sound is defined as $c = \sqrt{\gamma(p + \pi)/\rho}$.

$$\frac{1}{\gamma - 1} = \sum \frac{\alpha_i}{\gamma_i - 1} \tag{6}$$

$$\frac{\gamma \pi}{\gamma - 1} = \sum \frac{\alpha_i \gamma_i \pi_i}{\gamma_i - 1} \tag{7}$$

It is noted that the proof of hyperbolicity of the system in a quasi-linear form with primitive variables was made by Saurel and LeMetayer [24] and by Allaire et al. [15].

III. Results and Discussions

In this section, typical test problems such as gas–gas shock tube, water–air shock tube, and underwater explosion problems are considered to study the capability of our numerical method. Subsequently, we will discuss the evolution of stripping breakup of a water droplet by using the two-dimensional numerical simulation. The displacement, acceleration, volume change, and unsteady drag force of the water droplet will be investigated. In addition, the simulated results will be compared with the experimental results of Igra and Takayama [12].

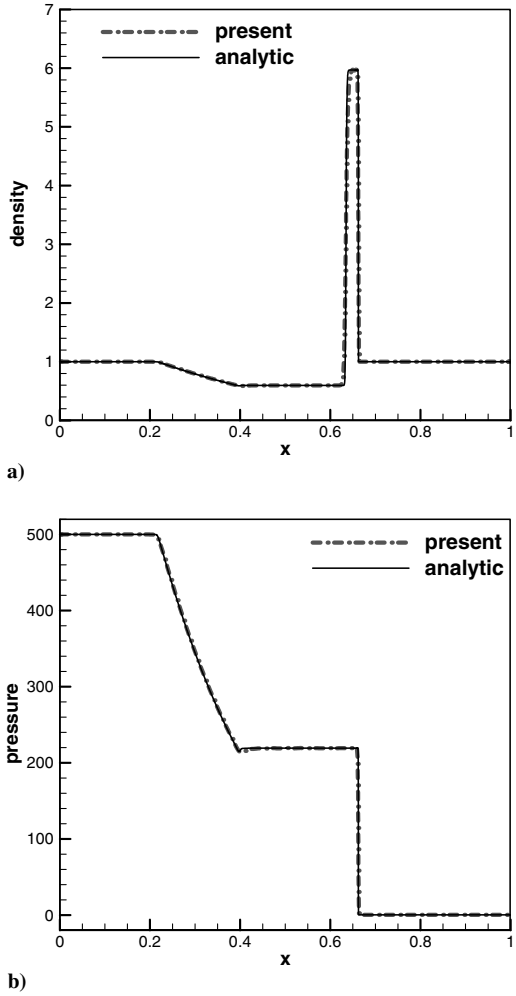

Fig. 2 Numerical results for gas–gas shock tube problem at $t = 0.01$.

A. Gas–Gas Shock Tube Problem

A strong-shock gas–gas shock tube problem is considered as our first test problem. The shock tube is one unit length and the diaphragm is located at $x = 0.5$. The initial conditions in the dimensionless form for the left and right states are $(\rho, u, p, \gamma)_L = (1, 0, 500, 1.6)$ and $(\rho, u, p, \gamma)_R = (1, 0, 0.2, 1.4)$, respectively. Figure 2 presents our numerical results. The presented results are obtained with a uniform grid of $\Delta x = 0.001$, and the Courant–Friedrichs–Lewy (CFL) number is 0.8 for this computation. As shown in Fig. 2, the presented results are in good agreement with analytic solutions. This problem consists of a very strong shock with a Mach number of 31 moving to the right and a rarefaction wave moving to the left. It can be seen that the shock front, contact surface, and rarefaction waves are sharply captured.

B. Water–Air Shock Tube Problem

The second test problem is a water–air shock tube problem. The length of the shock tube is 1 m. The diaphragm is located at $x = 0.7$ m. It has high-pressure liquid on the left-hand side and gas on the right-hand side. All fluids are at rest at $t = 0$. The initial conditions for water and air are

$$(\rho, p, \gamma, \pi)_w = (1000\ \text{kg/m}^3, 10^9\ \text{Pa}, 4.4, 6 \times 10^8\ \text{Pa})$$

and

$$(\rho, p, \gamma, \pi)_a = (50\ \text{kg/m}^3, 10^5\ \text{Pa}, 1.4, 0)$$

respectively. A large pressure ratio of 10^4 is imposed across the diaphragm. In our numerical simulations, two meshes with 200 and 1000 cells are used as coarse and fine grids, respectively. The CFL

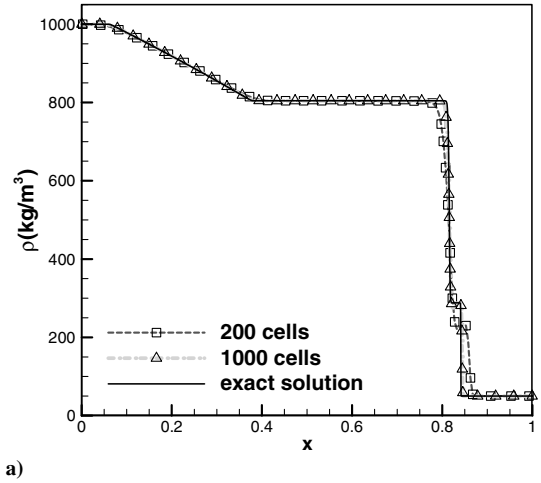

a)

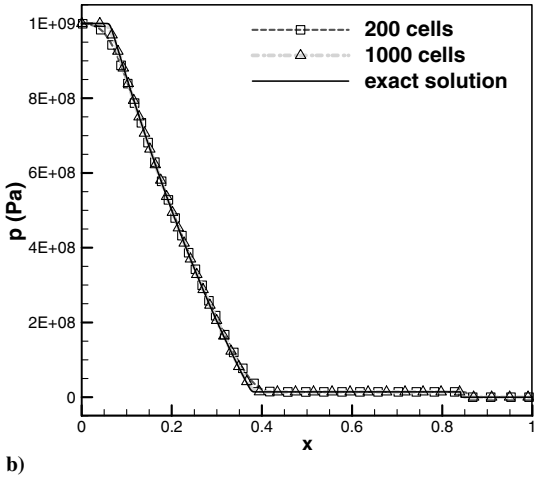

b)

Fig. 3 The comparison of water–air shock tube problem between present results and exact solutions at $t = 240$ μs.

number in this computation is chosen to be 0.8. In Fig. 3, the simulated result at $t = 240$ ms is presented. By comparing our results with the exact solutions, the correct positions of the contact surface, shock front, and rarefaction waves are shown. The computed mixture density and pressure for both coarse and fine grids are shown in Fig. 3. The presented results show good agreement with the exact solutions. In addition, the numerical errors are reduced as the mesh is refined.

C. Underwater Explosion Problem

The next test case is an underwater explosion problem. In this case, we followed the same numerical conditions of Shyue [25]. The computational domain is

$$\{(x, y)| -2 \le x \le 2, -1.5 \le y \le 1\} \text{ mm}$$

The initial condition includes a horizontal air–water interface at $y = 0$ axis and an underwater circular high-pressure gas bubble with the center $(x_0, y_0) = (0, -0.3)$ and a radius of 0.12 m. About the air–water interface, the fluid is a perfect gas:

$$(\rho, p, \gamma, \pi) = (1.225 \text{ kg/m}^3, 1.03125 \times 10^5 \text{ Pa}, 1.4, 0)$$

Below the air–water interface, the fluid is water:

$$(\rho, p, \gamma, \pi) = (10^3 \text{ kg/m}^3, 1.03125 \times 10^5 \text{ Pa}, 4.4, 6 \times 10^8 \text{ Pa})$$

Inside the gas bubble, the fluid is a perfect gas with high pressure:

$$(\rho, p, \gamma, \pi) = (1250 \text{ kg/m}^3, 10^9 \text{ Pa}, 1.4, 0)$$

Figure 4 shows the computed schlieren images at $t = 0.2$, 0.4, 0.8, and 1.2 ms. Note that the computed schlieren images presented in this

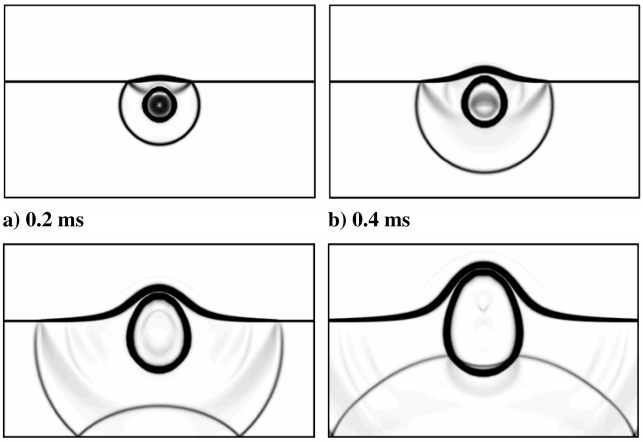

a) 0.2 ms b) 0.4 ms

c) 0.8 ms d) 1.2 ms

Fig. 4 Computed schlieren images for underwater explosion problem at different instants.

paper were created by using the magnitude of the density gradient $|\nabla\rho|$. Initially, due to the pressure difference between the high-pressure gas bubble and water, breakup of the gas bubble results in a circular shock wave propagating outward and a rarefaction wave propagating inward. After the circular shock wave interacts with the horizontal air–water interface, a reflected shock wave is formed and the air–water interface begins to deform. As time advances, the gas bubble continues moving upward, resulting in the subsequent deformation of the air–water interface.

It is noted that we did not use a tracking method here so that the presented results are only compared with the numerical results of Shyue [25] by using a mixture-type model equation with a nontracking method. In this problem, it includes the interface deformation, shock/interface interaction, and shock reflection. As shown in Fig. 4, it is found that our results are in agreement with Shyue's result [25]. Figure 5 shows the comparison of density distributions along $x = 0$ at $t = 0.4$ and 1.2 ms. It can be seen that the locations of interfaces and shock front agree well with the results of Shyue [25].

D. Stripping Breakup of a Water Droplet

1. Evolution of Stripping Breakup of a Water Droplet

Up to now, the evolution of stripping breakup of a water droplet has been studied by many experimental researchers. However, the stripping breakup of a water droplet is still unclear because of the restriction of experimental flow-visualization techniques.

To understand the mechanism of stripping breakup of a water droplet, the computed schlieren images for $Ms = 1.47$ is presented in Fig. 6, in which the shape of the water droplet is indicated by the white contour line of the water's volume fraction. In this study, the fluid interface is identified by the water's volume fraction α_w of 0.9. As shown in Fig. 6a, the incident shock S_I is going to impinge the water droplet at $t = 0$. At $t = 100$ ms, the shock/water-droplet interaction is completed. The reflected shock wave (RW) observed in the upstream is as a result of the incident shock reflecting from the front side (left-hand side) of the water droplet. The diffracted shock wave (DW) in the downstream is caused by the incident shock diffracting over the surface of the water droplet. A Mach reflection occurs due to the diffracted shock interacting with the incident shock; the corresponding Mach stem, primary vortex pair (VP) and two triple points (TP) are shown in Fig. 6b. Notably, the shape of the water droplet begins to be deformed due to the unbalanced pressure distribution acting on the surface. The rear side of the water droplet is going to be flattened. At $t = 200$ ms, the rear side of the water droplet reveals a concave shape. The shape of the water droplet is elongated in the lateral direction, but narrowed in the flow direction. In addition, the primary vortex pair is deformed and its profile becomes larger. Notably, two tips (T) are observed at this instant. A similar phenomenon has been reported by Wierzba and Takayama [1]. They

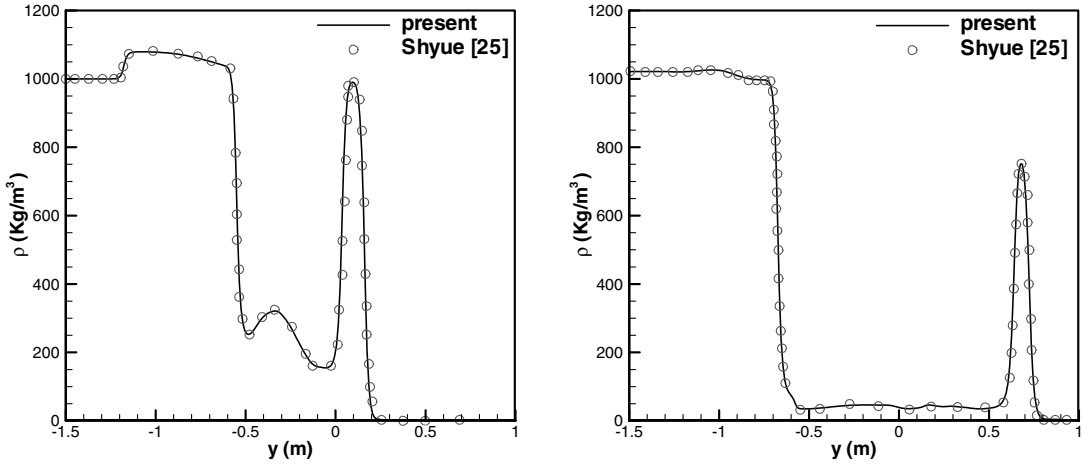

a) 0.4 ms **b) 1.2 ms**

Fig. 5 Comparison of density distribution along $x = 0$ at different instants.

mentioned that these two tips are the initial points of the stripping process. At $t = 300$ μs, the water droplet is deformed to be a crescentlike shape. The profile of the primary vortex pair becomes much larger. At this instant, an initial stage of vortex shedding is found in the downstream. It is straightforward to realize that the flowfield at the early stage of the stripping process is similar to the flow over a circular cylinder. For such a problem, the behavior of vortex shedding depends on its Reynolds number. It is noted that the shape of the water droplet is changing with time during the stripping process and the droplet is gradually disintegrating. These characteristics may result in differences to the typical vortex shedding. At $t = 400$ μs, it is found that the initial stage of vortex shedding occurs in the downstream, and the primary vortex structure becomes unstable. At $t = 500$ μs, the vortex shedding from the chaotic vortex structure near the rear of the droplet is clearly observed. In addition, the shape of the water droplet approximately reaches its maximum lateral deformation. Later, the shape of the water droplet disintegrates into two parts at $t = 600$ μs. Meanwhile, the vortex street becomes irregular. It can be seen that the vortex shedding is unstable at this instant. At $t = 700$ μs, the shape of the water droplet cannot be identified. The water droplet has disintegrated completely. Basically, the stripping breakup of a water droplet has terminated. It is noted that no small drop formed in the wake region is predicted in the present result using the inviscid-flow model, which is different from the result of Chou et al. [7] Furthermore, they mentioned that the sizes of small drops in the wake region are significantly affected by liquid viscosity.

Figure 7 shows the vorticity contours at $t = 200$ to 700 μs, corresponding to the same instants in Fig. 6. Figure 7a shows the vorticity contours with the primary and secondary vortex pair (second VP) at $t = 200$ μs. At $t = 300$ μs, the secondary vortex pair propagates downstream and merges into the primary vortex pair, resulting in instabilities inside the primary vortex structure. At $t = 400$ μs, a vortex-shedding phenomenon is observed, and the instabilities occur inside the primary vortex structure, resulting in the collapse of the primary vortex structure. At $t = 500$ μs, a vortex street can be observed clearly and the behavior of vortex shedding becomes unstable at this instant. Subsequently, the vortex street collapses due to the growth of flow instabilities at $t = 600$ μs. Later, the water droplet disintegrates and the primary vortex structure as totally collapses at $t = 700$ μs.

To understand the mechanism of the tip formation, Figs. 8 and 9 show the pressure and velocity contours at $t = 110$ and 150 μs, in which the shape of water droplet is indicated by the white contour line of $\alpha_w = 0.9$. In Fig. 8a, it is found that the high-pressure zones (HP) are at the front and rear sides of the droplet, but the low-pressure (LP) zones are at the upper and lower sides. The high pressure compresses the droplet in the flow direction, but the low pressure elongates the droplet in the lateral direction. Moreover, the unbalanced pressure distribution inside the water droplet also contributes to the shape deformation. As shown in Fig. 8b, the tips can be clearly seen. The locations of the two tips are related to the low-pressure zones. To show the detail of the velocity field, the velocity contours and vectors are both presented in Fig. 9. As shown in Fig. 9a, a high-speed (HS) zone corresponding to the low-pressure region in Fig. 8a is presented. In Fig. 9b, the high-speed zone propagates downstream and a secondary vortex pair (second VP) is formed, due to the shape deformation of the water droplet.

2. *Flow Instability*

As shown in Figs. 6 and 7, the flow instabilities are clearly observed. It is known that both Rayleigh–Taylor instability [26] (R–T instability) and Kelvin–Helmholtz instability [27] (K–H instability) play important roles in the liquid-droplet breakup. The R–T instability occurs while a dense, heavy fluid is being accelerated by a light fluid that is strongly dependent on the value of the acceleration a. Here, we introduce the Bond number B_o, which denotes the ratio of body force to surface tension force. It is defined as $B_o = a\rho_l D_o^2/4\sigma$. In our simulation, the Bond numbers $B_o = 2048$ and 4443 are less than 10^4. As defined by Harper et al. [28] for a quasi-stable droplet, B_o is less than 10^4. They also showed that the interfacial instability does not occur for a quasi-stable droplet. Therefore, we conclude that R–T instability is not the main reason for the droplet breakup in our problem. The K–H instability can occur when the velocity shear is present within a continuous fluid or when there is a sufficient velocity difference across the interface between two fluids. In our simulation, the vortex shedding basically is caused by the K–H instability. The unstable vortex shedding may result in varying force acting on the water-droplet surface. It may cause the oscillation of the water droplet, which is possibly related to the stripping breakup.

3. *Trajectory of the Water Droplet*

In this work, the location of a water droplet is defined based on the front end of the droplet. The displacements of the water droplet for $Ms = 1.3$ and 1.47 are shown in Fig. 10. To compare with the experimental results, the result of Igra and Takayama [12] is also presented in Fig. 10. As shown in Fig. 10a, the trend of the present numerical result is similar to the experimental one. It reveals that a higher Mach number can make the droplet move faster. Notably, the computed displacements are higher than those in the experimental result. The main reason for the difference is that the experimental result includes the effect of drag force between the optical window and water droplet, but it does not exist in our numerical simulation. Figure 10b shows the trends of dimensionless displacements, in which the dimensionless displacement and time are defined as $x^* = x/D_o$ and $t^* = t \cdot u_g/D_o$. It can be seen that our numerical results are close to the experimental results in dimensionless form and seem to fit a similar curve.

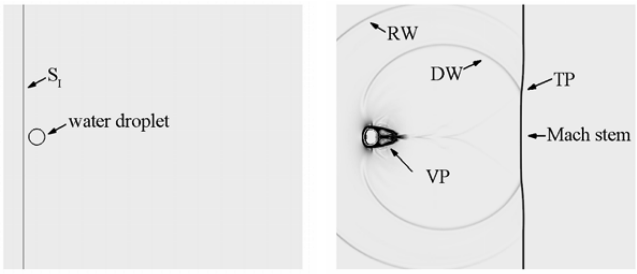

a) 0 μs b) 100 μs

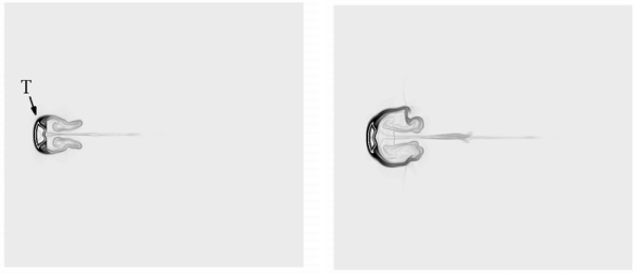

c) 200 μs d) 300 μs

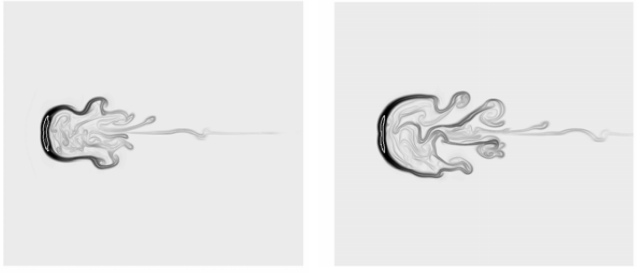

e) 400 μs f) 500 μs

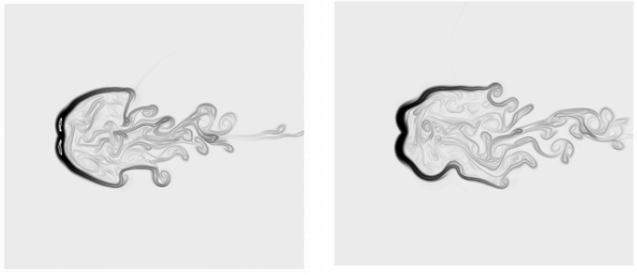

g) 600 μs h) 700 μs

Fig. 6 The computed schlieren images for $Ms = 1.47$ at different instants.

Figure 11 shows the acceleration history of the water droplet in the process of stripping breakup. In Fig. 11a, we can see that the trends of numerical and experimental results are similar. In the process of stripping breakup, it is found that the higher acceleration is induced at the early stage and then gradually decreases to a nearly constant value. In this study, the nearly constant acceleration of the water droplet approximates 14,000 m/s^2 for $Ms = 1.3$ and 54,000 m/s^2 for $Ms = 1.47$. The corresponding accelerations in the experiment of Igra and Takayama [12] are 13,700 and 34,035 m/s^2. As mentioned before, the reason for this difference is that the drag force between the optical window and water droplet in the experiments can offer a resistance against the force induced by the high-speed airstream. Comparing the numerical with the experimental results, it is found that the higher Mach number, the larger the difference. The dimensionless form of acceleration is presented in Fig. 11b. The dimensionless acceleration can be obtained directly from $x^* = a^* t^{*2}/2$. It is shown that the trends for all cases are similar. The dimensionless acceleration for $Ms = 1.3$ and 1.47 calculated

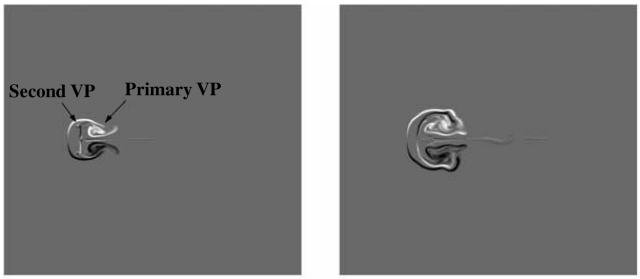

a) 200 μs b) 300 μs

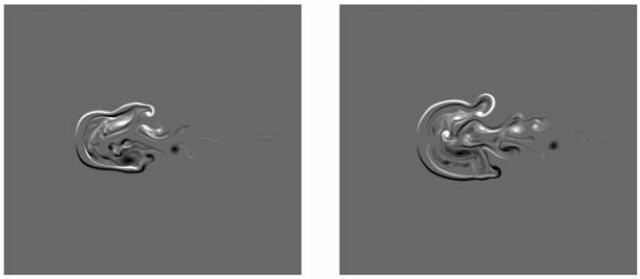

c) 400 μs d) 500 μs

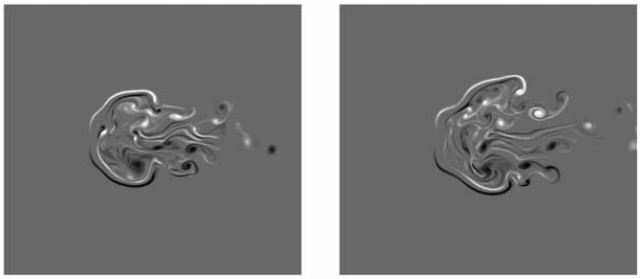

e) 600 μs f) 700 μs

Fig. 7 Vorticity contours for $Ms = 1.47$ at different instants.

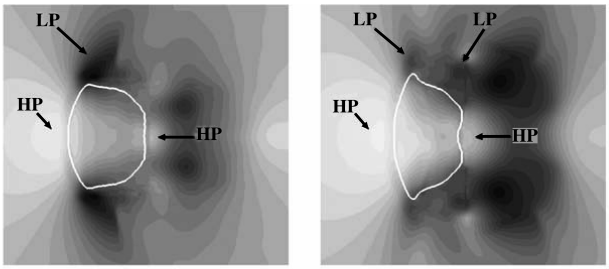

a) 110 μs b) 150 μs

Fig. 8 Pressure contours for $Ms = 1.47$; the light area denotes the high pressure: a) $t = 110$ μs and b) $t = 150$ μs.

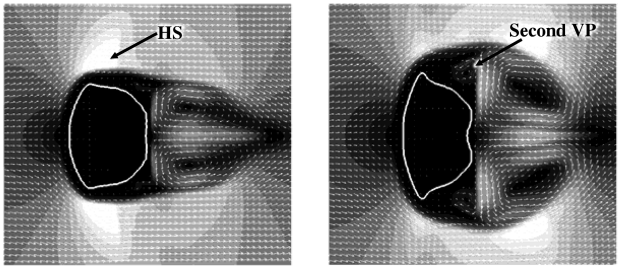

a) 110 μs b) 150 μs

Fig. 9 Velocity contours and velocity vectors for $Ms = 1.47$; the light area denotes the high velocity: a) $t = 110$ μs and b) $t = 150$ μs.

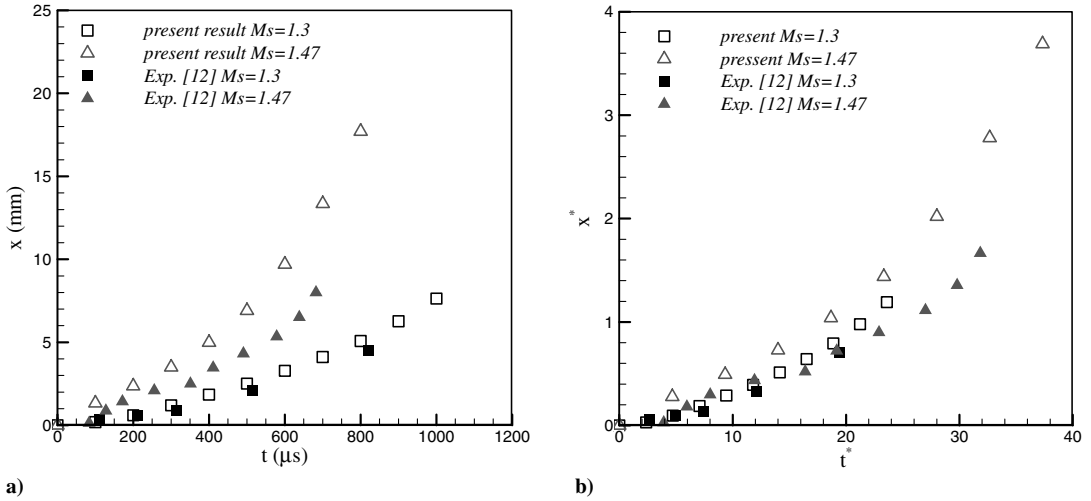

Fig. 10 Displacement history of a water droplet for $Ms = 1.3$ and 1.47 during the stripping breakup.

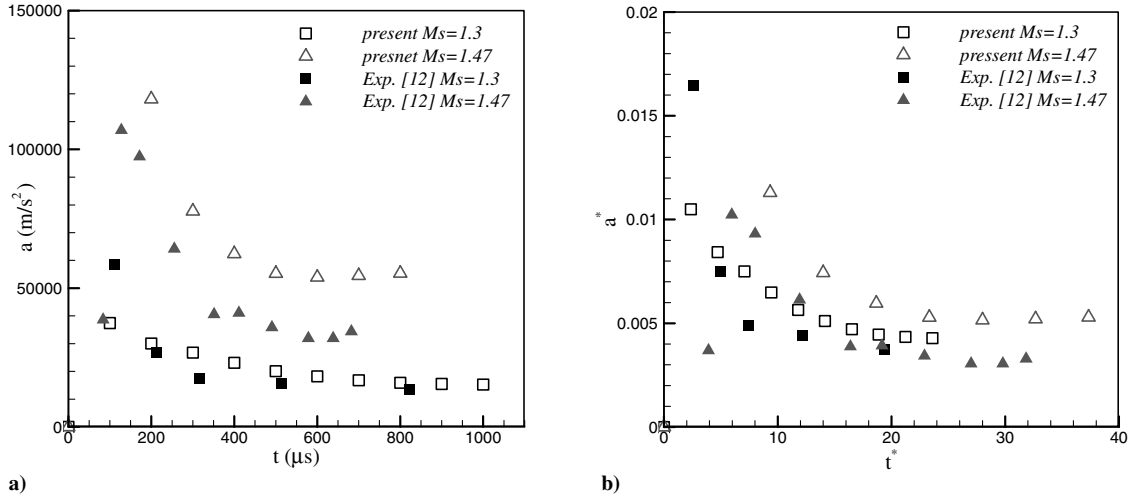

Fig. 11 Acceleration history of a water droplet during the stripping breakup.

from the numerical results are 0.00434 and 0.0052, and the corresponding experimental data are 0.004004 and 0.0033754. We infer that the difference is mainly due to the drag force between the optical window and water droplet in the experiment.

4. *Deformation of the Water Droplet*

The deformation of the water droplet in the stripping breakup is a significant issue. However, the exact profile of the deformed water droplet is still difficult to define. In this work, the shape of the deformed water droplet is defined by $\alpha_w = 0.9$. The history of the volume change in the dimensionless form is presented in Fig. 12. As shown in Fig. 12, the simulated curves are in agreement with the experimental data. Although the numerical curves are steeper than the experimental curves, the trends are basically similar. In Fig. 12, the variation of the slope shows that the stripping breakup at the later stage is more intense than that at the early stage. As shown in the zoom-in plot in Fig. 12, the oscillatory computed curves may imply that the shape of the water droplet in the stripping breakup is varying.

5. *Unsteady Drag Force*

Finally, an initial deformation of a water droplet from the point of view of unsteady drag force is presented. Figure 13 shows the temporal variation of computed unsteady drag coefficients. The drag force coefficient is defined as $C_d = F/(0.5\rho_g u_g^2 D_o)$, where F is the unsteady drag force. As shown in Fig. 13, the present result of unsteady drag coefficient is in agreement with the numerical result of Igra and Takayama [14] at the early stage of shock interaction with a water column. It is found that dimensionless times of peak pressure are very close in the present results. Basically, the unsteady drag force can be used to interpret the temporal variation of the

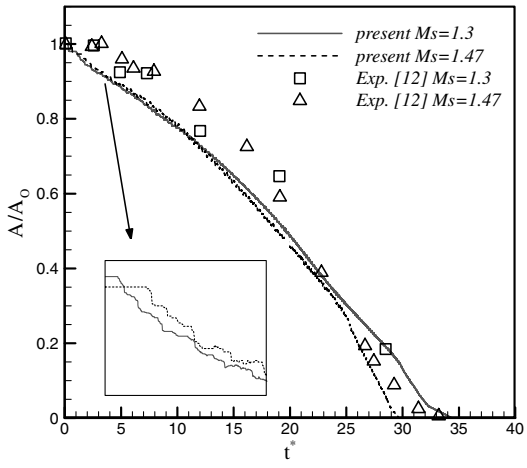

Fig. 12 Volume-change history of a water droplet in the dimensionless form during the stripping breakup.

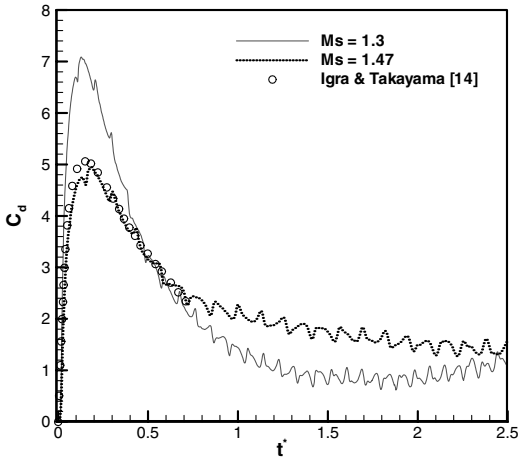

Fig. 13 Temporal variation of unsteady drag coefficients.

acceleration of droplet. In addition, the oscillation phenomenon of drag coefficient was also observed in the numerical result of Tanno et al. [13]. It is noted that the temporal variation of unsteady drag coefficients is different from that for the cylinder case when the droplet begins to deform.

IV. Conclusions

In this study, the evolution of the stripping breakup of a water droplet is simulated by using a multiphase flow solver with a five-equation model. To compare with the experimental results, the water droplets with diameters of 6.4 and 4.8 mm and $Ms = 1.3$ and 1.47 are chosen in this study. The stripping breakup of a water droplet, including the shape deformation, vortex shedding, flow instability, and unsteady drag force, is investigated. The computed displacement of the water droplet is in agreement with experimental data. It is found that all the numerical and experimental displacements in dimensionless form seem to fit a similar curve. In addition, the acceleration of the water droplet reaches its maximum value at the early stage and then gradually decreases to a nearly constant value. The volume-change history of the water droplet is shown in dimensionless form, and the trends of computed curves are similar to the experimental curves. Moreover, the evolution of a water droplet during the stripping breakup for an inviscid flow is presented by flow visualization.

Acknowledgments

The support for the work under the National Science Council contract NSC 96-2221-E-426-001 is gratefully acknowledged. The author would like to thank R. Saurel for his great help in code development and to also thank S. M. Liang for reading the manuscript.

References

[1] Wierzba, A., and Takayama, K., "Experimental Investigation of the Aerodynamic Breakup of Liquid Drops," *AIAA Journal*, Vol. 26, No. 11, 1988, pp. 1329–1335.

[2] Joseph, D. D., Belanger, J., and Beavers, G. S., "Breakup of a Liquid Suddenly Exposed to a High-Speed Airstream," *International Journal of Multiphase Flow*, Vol. 25, Nos. 6–7, 1999, pp. 1263–1303. doi:10.1016/S0301-9322(99)00043-9

[3] Pilch, M., and Erdman, C. A., "Use of Break-Up Time Data and Velocity History Data to Predict the Maximum Size of Stable Fragments for Acceleration-Induced Breakup of a Liquid Drop," *International Journal of Multiphase Flow*, Vol. 13, No. 6, 1987, pp. 741–757. doi:10.1016/0301-9322(87)90063-2

[4] Hirahara, H., and Kawahashi, M., "Experimental Investigation of Viscous Effects upon a Breakup of Droplets in High-Speed Air Flow," *Experiments in Fluids*, Vol. 13, No. 6, 1992, pp. 423–428. doi:10.1007/BF00223250

[5] Ranger, A. A., and Nicholls, J. A., "Aerodynamic Shattering of Liquid Drops," *AIAA Journal*, Vol. 7, No. 2, 1969, pp. 285–290.

[6] Yoshida, T., and Takayama, K., "Interaction of Liquid Droplets with Planar Shock Waves," *Journal of Fluids Engineering*, Vol. 112, No. 4, 1990, pp. 481–486.

[7] Chou, W.-H., Hsiang, L.-P., and Faeth, G. M., "Temporal Properties of Drop Breakup in the Shear Breakup Regime," *International Journal of Multiphase Flow*, Vol. 23, No. 4, 1997, pp. 651–669. doi:10.1016/S0301-9322(97)00006-2

[8] Theofanous, T. G., Li, G. J., and Dinh, T. N., "Aerobreakup in Rarefied Supersonic Gas Flows," *Journal of Fluids Engineering*, Vol. 126, No. 4, 2004, pp. 516–527. doi:10.1115/1.1777234

[9] Igra, D., and Takayama, K., "Investigation of Aerodynamic Breakup of a Cylindrical Water Droplet," *Reports of the Institute of Fluid Science, Tohoku University*, Vol. 11, 1999, pp. 123–134.

[10] Igra, D., and Takayama, K., "Numerical Simulation of Shock Wave Interaction with a Water Column," *Shock Waves*, Vol. 11, No. 3, 2001, pp. 219–228. doi:10.1007/PL00004077

[11] Igra, D., and Takayama, K., "Investigation of Aerodynamic Breakup of a Cylindrical Water Droplet," *Atomization and Sprays*, Vol. 11, No. 2, 2001, pp. 167–185.

[12] Igra, D., and Takayama, K., "A Study of Shock Wave Loading on a Cylindrical Water Column," *Reports of the Institute of Fluid Science, Tohoku University*, Vol. 13, 2001, pp. 19–36.

[13] Tanno, H., Itoh, K., Saito, T., Abe, A., and Takayama, K., "Interaction of a Shock with a Sphere Suspended in a Vertical Shock Tube," *Shock Waves*, Vol. 13, No. 3, 2003, pp. 191–200. doi:10.1007/s00193-003-0209-y

[14] Igra, D., and Takayama, K., "Experimental Investigation of Two Cylindrical Water Columns Subjected to Planar Shock Wave Loading," *Journal of Fluids Engineering*, Vol. 125, No. 2, 2003, pp. 325–331. doi:10.1115/1.1538628

[15] Allaire, G., Clerc, S., and Kokh, S., "A Five-Equation Model for Simulation of Interfaces Between Compressible Fluids," *Journal of Computational Physics*, Vol. 181, No. 2, 2002, pp. 577–616. doi:10.1006/jcph.2002.7143

[16] Perigaud, G., and Saurel, R., "A Compressible Flow Model with Capillary Effects," *Journal of Computational Physics*, Vol. 209, No. 1, 2005, pp. 139–178. doi:10.1016/j.jcp.2005.03.018

[17] Harten, A., Lax, P. D., and van Leer, B., "On Upstream Differencing and Godunov-Type Schemes for Hyperbolic Conservation Laws," *SIAM Review*, Vol. 25, No. 1, 1983, pp. 35–61. doi:10.1137/1025002

[18] Toro, E. F., Spruce, M., and Spears, W., "Restoration of the Contact Surface in the HLL-Riemann Solver," *Shock Waves*, Vol. 4, No. 1, 1994, pp. 25–34. doi:10.1007/BF01414629

[19] Saurel, R., and Abgrall, R., "A Multiphase Godunov Method for Compressible Multifluid and Multiphase Flows," *Journal of Computational Physics*, Vol. 150, No. 2, 1999, pp. 425–467. doi:10.1006/jcph.1999.6187

[20] Saurel, R., and Abgrall, R., "A Simple Method for Compressible Multifluid Flows," *SIAM Journal on Scientific Computing*, Vol. 21, No. 3, 1999, pp. 1115–1145. doi:10.1137/S1064827597323749

[21] Shyue, K.-M., "A Fluid Mixture Type Algorithm for Compressible Multicomponent Flow with van der Waals Equation of State," *Journal of Computational Physics*, Vol. 156, No. 1, 1999, pp. 43–88. doi:10.1006/jcph.1999.6349

[22] Shyue, K.-M., "A Fluid-Mixture Type Algorithm for Barotropic Two-Fluid Flow Problems," *Journal of Computational Physics*, Vol. 200, No. 2, 2004, pp. 718–748. doi:10.1016/j.jcp.2004.05.003

[23] Shyue, K.-M., "A Fluid Mixture-Type Algorithm for Compressible Multicomponent Flow with Mie-Grüneisen Equation of State," *Journal of Computational Physics*, Vol. 171, No. 2, 2001, pp. 678–707. doi:10.1006/jcph.2001.6801

[24] Saurel, R., and LeMetayer, O., "A Multiphase Model for Compressible Flows with Interfaces, Shocks, Detonation Waves and Cavitation," *Journal of Fluid Mechanics*, Vol. 431, No. 6, 2001, pp. 239–271. doi:10.1017/S0022112000003098

[25] Shyue, K-M., "A Wave-Propagation Based Volume Tracking Method for Compressible Multicomponent Flow in Two Space Dimensions," *Journal of Computational Physics*, Vol. 215, No. 1, 2006, pp. 219–244. doi:10.1016/j.jcp.2005.10.030

[26] Taylor, G. I., "The Instability of Liquid Surfaces When Accelerated in a Direction Perpendicular to Their Planes," *Proceedings of the Royal Society of London Series A*, Vol. 201, No. 1065, 1950, pp. 192–196.
[27] Kelvin, W. T., "Hydrokinetic Solutions and Observations," *Philosophical Magazine*, Vol. 42, 1871, pp. 362–377.
[28] Harper, E. Y., Grube, G. W., and Chang, I.-D., "On The Breakup of Accelerating Liquid Drops," *Journal of Fluid Mechanics*, Vol. 52, No. 3, 1972, pp. 565–591.
doi:10.1017/S0022112072001594

R. Rangel
Associate Editor